Fine Structure of Short-Lived States of Hydrogen by a Microwave-Optical Method. I*

W. E. LAMB, JR.,† AND T. M. SANDERS, JR.‡
Department of Physics, Stanford University, Stanford, California
(Received April 15, 1960)

A radio-frequency determination of the fine structure of excited states of hydrogen atoms is described. In this method the atoms are excited by electron bombardment so that they emit radiation. Transitions among the fine structure levels are induced by a radio-frequency electric field and are detected by the consequent change in intensity of the emitted radiation. A detailed theory of the method is presented and the experimental apparatus is discussed and described. Some preliminary results for the $n=3$ level of deuterium are: $\Delta E-\delta=2934.5\pm10$ Mc/sec, $\delta=316.3\pm10$ Mc/sec, where ΔE is the separation $3\,^2P_{\frac{1}{2}}-3\,^2P_{\frac{3}{2}}$, and δ the separation $3\,^2S_{\frac{1}{2}}-3\,^2P_{\frac{1}{2}}$; these results are in agreement with predictions of quantum electrodynamics.

INTRODUCTION

IN an earlier note,[1] an account was given of the use of a microwave-optical method to study the fine structure of hydrogen in the excited states $n=3$. These states are of interest because the quantum electrodynamical level shifts are predicted by theory to depend in a peculiar logarithmic fashion on the principal quantum number n. Previous spectroscopic observations[2] on $n=3$ have indicated the possibility of a discrepancy with theory, and in any case, the ultimate accuracy of such observations leaves much to be desired. Furthermore, there are still small unexplained differences between observed and calculated shifts for the $n=2$ states of hydrogen and singly ionized helium.[3] It is hoped that the present study might give a clue to the origin of these discrepancies.

The method involves excitation of hydrogen atoms to the $n=3$ states, $3s$, $3p$, and $3d$ by a low-energy electron beam and observation of the Balmer α radiation which is emitted in transitions $3s\rightarrow 2p$, $3p\rightarrow 2s$ and $3d\rightarrow 2p$. Atoms in the $3s$ and $3d$ levels can decay to lower states only with emission of Balmer α light, but while atoms in $3p$ can emit that radiation, they are 7.5 times more likely to emit the ultraviolet Lyman β radiation and decay to $1s$. The levels $3s$, $3p$, $3d$ are unequally populated by electron bombardment; hence, it is possible to change the intensity of Balmer α (or Lyman β) radiation by application of radio waves which cause transitions $3s\leftrightarrow 3p$ or $3d\leftrightarrow 3p$ before the excited atoms can decay. The desired energy separations can be obtained from the radio frequencies which produce such changes in optical intensity.

Although applied here to the $n=3$ levels of deuterium, the method can clearly be adapted to other states of hydrogen-like systems, and can be regarded as a generalization of the method used by Lamb and Skinner[4] for $n=2$ of ionized helium.

In part A of this paper we given the theory underlying the measurements described in part C. In part B the design of the experimental apparatus is discussed. Since the theoretical complexities multiply rapidly as one strives for precision, no systematic effort will be made to deal with terms smaller than 0.1 Mc/sec.

A. THEORY

1. Signal Due to Induced Transitions, Rate Treatment

For simplicity, the case of two decaying levels will be treated first. Let us consider an isolated system having two excited states a and b with lifetimes for radiative decay to lower states $\tau_a=1/\gamma_a$ and $\tau_b=1/\gamma_b$, respectively. For instance, a might be one of the $3s$ sublevels and b one of those for $3p$ of atomic hydrogen. Let atoms be excited to these states by electron bombardment at rates r_a and r_b, and let some perturbation such as an rf electric field cause transitions between the excited states. Plausible differential equations can then be written for the numbers n_a and n_b of atoms in the excited states

$$\begin{aligned}\dot{n}_a&=r_a-\gamma_a n_a+W(n_b-n_a),\\ \dot{n}_b&=r_b-\gamma_b n_b+W(n_a-n_b).\end{aligned}\tag{1}$$

It is assumed here that the only effect of the rf perturbation is to cause transitions between a and b which can be described by a rate constant W. Usually rather special assumptions (e.g., existence of a continuum of initial or final states of suitable energy) have to be

* This work was supported by the Office of Naval Research.
† Present address: Oxford University, Oxford, England.
‡ Present address: School of Physics, University of Minnesota, Minneapolis, Minnesota.
[1] W. E. Lamb, Jr., and T. M. Sanders, Jr., Phys. Rev. **103**, 313 (1956).
[2] G. W. Series, Proc. Roy. Soc. (London) **A208**, 277 (1951).
[3] C. M. Sommerfield, Phys. Rev. **107**, 328 (1957). A. Petermann, Fortschr. Physik **6**, 505 (1958). For a recent evaluation see A. J. Layzer, Phys. Rev. Letters **4**, 580 (1960).
[4] The earlier papers on radio-frequency fine structure measurements in the $n=2$ levels of hydrogen, deuterium, and ionized helium will be cited frequently in the text. The papers are listed here, along with abbreviated designations used in the text. H,D: W. E. Lamb, Jr., and R. C. Retherford, Phys. Rev. **72**, 241 (1947); **79**, 549 (1950)—L.R.-I; **81**, 222 (1951)—L.R.-II; **86**, 1014 (1952). W. E. Lamb, Jr., Phys. Rev. **85**, 259 (1952)—L.R.-III; S. Triebwasser, E. S. Dayhoff, and W. E. Lamb, Jr., Phys. Rev. **89**, 98 (1953); E. S. Dayhoff, S. Triebwasser, and W. E. Lamb, Jr. Phys. Rev. **89**, 106 (1953). He^+: W. E. Lamb, Jr., and M. Skinner, Jr., Phys. Rev. **78**, 539 (1950); R. Novick, E. Lipworth, and P. F. Yergin, Phys. Rev. **100**, 1153 (1955); E. Lipworth and R. Novick, Phys. Rev. **108**, 1434 (1957).

made in time-dependent perturbation theory in order to obtain transitions with a probability proportional to the time.[5] One might therefore doubt the validity of (1). The discussion in Sec. 2 shows, however, that Eqs. (1) are applicable under the conditions obtaining in the experiments.

In a steady state, $\dot{n}_a=\dot{n}_b=0$, and the relations

$$n_a=\frac{r_a\gamma_b+W(r_a+r_b)}{\gamma_a\gamma_b+W(\gamma_a+\gamma_b)},\qquad n_b=\frac{r_b\gamma_a+W(r_a+r_b)}{\gamma_a\gamma_b+W(\gamma_a+\gamma_b)},\tag{2}$$

give the stationary populations of excited atoms.

The atoms in states a, b undergo spontaneous transitions to lower states with decay rates γ_a, γ_b, respectively. Let f_a and f_b be the fractions of these decays which lead to radiation of the type detected (e.g., Balmer α). The rate of emission of these quanta is

$$r(W)=f_a\gamma_a n_a+f_b\gamma_b n_b,\tag{3}$$

and the change caused by turning off the rf power, or "signal" is

$$S=r(W)-r(0)=-(f_a-f_b)\left(\frac{r_a}{\gamma_a}-\frac{r_b}{\gamma_b}\right)W\Big/\left[1+\frac{W(\gamma_a+\gamma_b)}{\gamma_a\gamma_b}\right].\tag{4}$$

The first factor (f_a-f_b) indicates that a nonvanishing signal requires a difference in branching ratios; if both states a and b emit Balmer α equally, an rf-induced transition between them will produce no signal. The second factor

$$[(r_a/\gamma_a)-(r_b/\gamma_b)]$$

indicates that, unless the unperturbed steady-state populations of a and b are different, transitions $a\rightarrow b$ and $b\rightarrow a$ will exactly compensate, and again there will be no signal. The last factor gives the dependence of signal on the postulated rate constant W for rf-induced transitions between a and b. The signal S is proportional to the rf transition rate W for small W, but a saturation occurs for large W due to the effect of reverse rf-induced transitions.

The present treatment does not determine the dependence of W on rf amplitude, polarization, and frequency. We show in the next section that under certain reasonable assumptions we obtain

$$W=\tfrac{1}{4}(\gamma_a+\gamma_b)|V|^2/[(\nu-\omega)^2+\tfrac{1}{4}(\gamma_a+\gamma_b)^2].\tag{5}$$

Here $\hbar V$ is a matrix element of the interaction energy between atom and rf field, ν is the rf circular frequency, and $\omega>0$ is the resonance circular frequency. For the case $\gamma_a=0$, this agrees with the expression used in L.R.-I.

With W of Eq. (5) substituted into (4), the signal becomes

$$S=-(f_a-f_b)[(r_a/\gamma_a)-(r_b/\gamma_b)](\gamma_a+\gamma_b)\times\tfrac{1}{4}|V|^2\times[(\nu-\omega)^2+\tfrac{1}{4}(\gamma_a+\gamma_b)^2+\tfrac{1}{4}(\gamma_a+\gamma_b)^2|V|^2/\gamma_a\gamma_b]^{-1}.\tag{6}$$

The resonance curve is Lorentzian in shape, with center at $\nu=\omega$, and with width at half height,

$$(\gamma_a+\gamma_b)[1+|V|^2/\gamma_a\gamma_b]^{\frac{1}{2}}$$

in circular frequency units. For small rf power, the width is just the sum of the radiative widths of the two states a and b. For high rf power saturation occurs; the signal no longer increases linearly with rf power, and the resonance is broadened. For 50% saturation, $|V|^2=\gamma_a\gamma_b$, the signal at resonance is 50% of its maximum possible value and the resonance curve has a width at half height of $2^{\frac{1}{2}}(\gamma_a+\gamma_b)$. We will refer to the rf field strength sufficient to produce this condition as "optimum."

2. Justification of Rate Equations

Let us consider atoms excited to state a by electron bombardment at time t_0 so that the initial wavefunction is

$$\psi(\mathbf{r},t_0)=u_a(\mathbf{r}).\tag{7}$$

Due to rf perturbations and radiative decay, the wave function describing the excited atom at later times is a linear combination of the form

$$\psi(\mathbf{r},t)=a(t,t_0)u_a(\mathbf{r})e^{-iE_at/\hbar}+b(t,t_0)u_b(\mathbf{r})e^{-iE_bt/\hbar}.\tag{8}$$

The wave equations for $a(t,t_0)$ and $b(t,t_0)$ may be written as

$$i(da/dt)=V_{ab}(t)e^{i\omega t}b-(i/2)\gamma_a a,\qquad i(db/dt)=V_{ba}(t)e^{-i\omega t}a-(i/2)\gamma_b b,\tag{9}$$

where $\hbar V_{ab}(t)$ is the matrix element for transition $b\rightarrow a$ of the interaction energy $[\hbar V(t)=e\mathbf{E}(t)\cdot\mathbf{r}]$ of the rf field with the atom. The damping terms are introduced phenomenologically, but their form can be justified by a more detailed quantum-electrodynamic treatment.[6] The initial conditions are $a(t_0,t_0)=1$, $b(t_0,t_0)=0$. The probability that an atom is in state a at time t is $|a(t,t_0)|^2$, and, because of damping, falls off in a generally exponential manner for $t>t_0$, with pulsations caused by the rf-induced transitions $a\leftrightarrow b$. Since both of these changes in time take place over many periods of the emitted light, we may take

$$\gamma_a|a(t,t_0)|^2$$

to be the rate of spontaneous transitions at time t from state a for an atom put in state a at time t_0. There is a

[5] See, for example, L. I. Schiff, *Quantum Mechanics* (McGraw-Hill Book Company, Inc., New York, 1949), 1st ed., p. 192.

[6] V. Weisskopf and E. Wigner, Z. Physik **63**, 54 (1930).

corresponding rate at time t of radiative transitions from state b of $\gamma_b|b(t,t_0)|^2$. As the transitions $3s\rightarrow 2p$ and $3p\rightarrow 2s$ are incoherent processes, there is no interference. If atoms are excited to state a at a constant rate r_a, the steady rate of emission of detected light is

$$r_a\left[f_a\gamma_a\int_{-\infty}^{t}|a(t,t_0)|^2dt_0+f_b\gamma_b\int_{-\infty}^{t}|b(t,t_0)|^2dt_0\right],$$

where f_a and f_b are the branching ratios used previously. To obtain the total rate of emission of detected light, this must be supplemented by a similar expression to allow for contributions from atoms excited to state b at a rate r_b.

It is possible, although exceedingly tedious, to carry out the indicated operations on the transient solutions $a(t,t_0)$, $b(t,t_0)$ of the time-dependent wave equations, and to derive the resonance formula [Eq. (6)]. Instead, we give a simpler procedure[7] which makes direct use of the steady-state character of the problem, and which indicates how the rate treatment may be justified.

From Eq. (9), one can derive differential equations for the bilinear expressions a^*a, a^*b, ab^* and b^*b which are elements of a 2×2 density matrix. Thus

$$\begin{aligned}i(d/dt)(a^*a)&=V_{ab}e^{i\omega t}a^*b-V_{ba}e^{-i\omega t}ab^*-i\gamma_a a^*a,\\ i(d/dt)(a^*b)&=V_{ab}e^{-i\omega t}a^*a-V_{ba}e^{-i\omega t}b^*b\\ &\quad-(i/2)(\gamma_a+\gamma_b)a^*b,\end{aligned}\tag{10}$$

with similar equations for ab^* and b^*b. In these equations, a and b are subjected to the same initial conditions as before. In the experiment we are not interested in following the time dependence of the probabilities $|a(t,t_0)|^2$ and $|b(t,t_0)|^2$, but in the behavior at time t of an ensemble of atoms which were excited independently of each other to states a and b at rates r_a and r_b, respectively, for all times $t_0<t$. At this point we leave mechanistic quantum theory and consider an "ensemble in excitation and decay" described by a statistical density matrix $\sigma^{(a)}$ with elements such as

$$\begin{aligned}\sigma_{aa}{}^{(a)}(t)&=r_a\int_{-\infty}^{t}|a(t,t_0)|^2dt_0,\\ \sigma_{ab}{}^{(a)}(t)&=r_a\int_{-\infty}^{t}a^*(t,t_0)b(t,t_0)dt_0.\end{aligned}\tag{11}$$

The diagonal element $\sigma_{aa}{}^{(a)}$ represents the population of state a at time t which arises from a prolonged previous excitation of state a at rate r_a, while $\sigma_{bb}{}^{(a)}$ is the corresponding population of b. The off-diagonal elements such as $\sigma_{ba}{}^{(a)}$ have no simple interpretation in the present microwave-optical experiments. The time derivative of $\sigma_{aa}{}^{(a)}(t)$ is

$$(d/dt)\sigma_{aa}{}^{(a)}(t)=r_a+r_a\int_{-\infty}^{t}(d/dt)|a(t,t_0)|^2dt,\tag{12}$$

since $a(t_0,t_0)=1$, but in the corresponding equations for time derivatives of $\sigma_{bb}{}^{(a)}$, $\sigma_{ba}{}^{(a)}$ and $\sigma_{ab}{}^{(a)}$ the first term on the right is missing. When both states a and b are excited, the density matrix becomes

$$\sigma=\sigma^{(a)}+\sigma^{(b)}.$$

Its elements obey differential equations

$$(d/dt)\sigma_{aa}=r_a-iV_{ab}e^{i\omega t}\sigma_{ba}+iV_{ba}e^{-i\omega t}\sigma_{ab}-\gamma_a\sigma_{aa},\tag{13}$$

$$(d/dt)\sigma_{ba}=iV_{ba}e^{-i\omega t}(\sigma_{bb}-\sigma_{aa})-\tfrac{1}{2}(\gamma_a+\gamma_b)\sigma_{ba},\tag{14}$$

$$(d/dt)\sigma_{ab}=-iV_{ab}e^{i\omega t}(\sigma_{bb}-\sigma_{aa})-\tfrac{1}{2}(\gamma_a+\gamma_b)\sigma_{ab},\tag{15}$$

$$(d/dt)\sigma_{bb}=r_b-iV_{ba}e^{-i\omega t}\sigma_{ab}+iV_{ab}e^{i\omega t}\sigma_{ba}-\gamma_b\sigma_{bb}.\tag{16}$$

We now assume that an oscillating rf field of form $\mathbf{E}\cos\nu t$ acts on the system. As in the Rabi[8] theory of molecular beam resonances, it suffices for most applications to consider only the "rotating" parts of this field which are in resonance with the atomic transition. For $\nu>0$ this means that one should take

$$V_{ab}=(V/2)e^{-i\nu t}\quad\text{and}\quad V_{ba}=(V^*/2)e^{i\nu t}\tag{17}$$

where

$$V=e\mathbf{E}\cdot\mathbf{r}_{ab}/\hbar.\tag{18}$$

The extension analogous to the Bloch-Siegert[9] treatment will be given elsewhere. Under the assumption of a slowly-varying difference in population $(\sigma_{aa}-\sigma_{bb})$, we find from Eq. (14) the expression

$$\sigma_{ba}=(i/2)V\{(\sigma_{bb}-\sigma_{aa})/[i(\nu-\omega)+\tfrac{1}{2}(\gamma_a+\gamma_b)]\}\times e^{i(\nu-\omega)t},\tag{19}$$

apart from transient terms. Insertion of the off-diagonal elements of σ into Eq. (13) and Eq. (16) leads to equations for the diagonal elements σ_{aa} and σ_{bb}

$$\begin{aligned}(d/dt)\sigma_{aa}&=r_a-\gamma_a\sigma_{aa}+W(\sigma_{bb}-\sigma_{aa}),\\ (d/dt)\sigma_{bb}&=r_b-\gamma_b\sigma_{bb}+W(\sigma_{aa}-\sigma_{bb}),\end{aligned}\tag{20}$$

where

$$W=\tfrac{1}{4}(\gamma_a+\gamma_b)|V|^2/[(\nu-\omega)^2+\tfrac{1}{4}(\gamma_a+\gamma_b)^2].$$

These equations are exactly equivalent to those used in the rate treatment of Sec. 1. For the validity of the equations it was necessary to assume (1) the rotating field approximation, and (2) that the population difference $(\sigma_{aa}-\sigma_{bb})$ was slowly varying. These assumptions are valid for a steady-state experiment unless excessive rf is used.

Generalizations of this theory for cases of more than two levels will be given where needed in the following paper.

3. Energy Levels for $n=3$

The Dirac electron theory of 1928 predicted energy levels of $n=3$ of hydrogen is shown in Fig. 1(A). Levels with the same inner quantum number j were

[7] The utility of this method was suggested to the authors by F. Bloch.

[8] I. I. Rabi, Phys. Rev. **51**, 652 (1937).

[9] F. Bloch and A. Siegert, Phys. Rev. **57**, 522 (1940).

TABLE I. Contributions to the theoretical values of the level separations (a) $\mathcal{S}(3\,^2S_{\frac{1}{2}}-3\,^2P_{\frac{1}{2}})$, (b) $\Sigma(3\,^2P_{\frac{1}{2}}-3\,^2D_{\frac{1}{2}})$, (c) $\Delta E(3\,^2P_{\frac{1}{2}}-3\,^2P_{\frac{3}{2}})$, and (d) $\mathfrak{D}E(3\,^2D_{\frac{1}{2}}-3\,^2D_{\frac{3}{2}})$ in deuterium, and their values in megacycles per second.

(a) Contributions to $\mathcal{S}(3\,^2S_{\frac{1}{2}}-3\,^2P_{\frac{1}{2}})$	
Dirac:	
0	
Second order radiative shift:	
$(8/27)L(1-3m/M)\left(2\ln\alpha^{-1}+m/M+11/24+\ln\frac{k_0(3,1)}{k_0(3,0)}\right)$	300.89
Second order vacuum polarization:	
$(8/27)L(1-3m/M)(-1/5)$	−8.03
Second order magnetic moment:	
$(8/27)L(1-2.75m/M)(+1/2)$	+20.08
Second order relativistic shift:	
$(8/27)L(1-3m/M)(3\pi\alpha)(1+11/128-\frac{1}{2}\ln 2+5/192)$	+2.11
Fourth order radiative shift:	
$(8/27)L(3\alpha/2\pi)(0.52)$	+0.07
Fourth order vacuum polarization:	
$(8/27)L(-41\alpha/54\pi)$	−0.07
Fourth order magnetic moment:	
$(8/27)L(-0.328\alpha/\pi)$	−0.03
Finite-mass effect:	
$(8/27)L(m/M)(5.3684)$	+0.06
Finite-size effect for deuteron	
$(8/27)(\alpha^2/6)cR(mc/\hbar)^2\langle r^2\rangle_D$	+0.25
Total splitting	$\mathcal{S}=$ 315.33 Mc/sec
(b) Contributions to $\Sigma(3\,^2P_{\frac{1}{2}}-3\,^2D_{\frac{1}{2}})$	
Dirac:	
0	0
Second-order radiative shift:	
$(8/27)L\ln\left(\frac{k_0(3,2)}{k_0(3,1)}\right)$	1.32
Anomalous magnetic moment:	
$(8/27)L(3/8)[1/6+1/10]$	4.02
Total splitting	$\Sigma=$ 5.34 Mc/sec
(c) Contributions to $\Delta E(3\,^2P_{\frac{1}{2}}-3\,^2P_{\frac{3}{2}})$	
Dirac:	
$(cR\alpha^2/54)[1-(31/48)(\alpha Z)^2+\cdots]$	3243.10
Anomalous magnetic moment:	
$(8/27)L(3/16)\left(1-\frac{2m}{M}\right)\left(1-\frac{0.656\alpha}{\pi}\right)$	7.52
Total splitting	$\Delta E=$3250.62 Mc/sec
(d) Contributions to $\mathfrak{D}E(3\,^2D_{\frac{1}{2}}-3\,^2D_{\frac{3}{2}})$	
Dirac:	
$(cR\alpha^2/162)[1+(25/144)(\alpha Z)^2+\cdots]$	1081.08
Anomalous magnetic moment:	
$(8/27)L(3/8)(1/6)\left(1-\frac{2m}{M}\right)\left(1-\frac{0.656}{\pi}\right)$	2.51
Total splitting	$\mathfrak{D}E=$1083.59 Mc/sec
Constants used:	
$R=R_D=109\,707.419\pm0.012$ cm^{-1},	
$c=299\,793.0\pm0.3$ km sec^{-1},	
$\alpha^{-1}=137.0390\pm0.0012$,	
$L=(\alpha^3R_\infty c/3\pi)=135.6351\pm0.003$ Mc/sec.	

degenerate. After 1947, with the discovery of electromagnetic level shifts and the anomalous magnetic moment of the electron, it became necessary to modify the Dirac treatment. The effect of these corrections is to remove the degeneracy with respect to j, so that the level scheme for $n=3$ must be characterized by four parameters, $\mathcal{S}$, ΔE, Σ, and $\mathfrak{D}E$ as shown in Fig. 1(B).

The contributions to the separation $\mathcal{S}(3\,^2S_{\frac{1}{2}}-3\,^2P_{\frac{1}{2}})$ which have been calculated are shown in Table I(a). The frequency unit $L=\alpha^3cR_\infty/3\pi$ is Bethe's level shift constant. The main n^{-3} dependence of these terms is given by the common factor (8/27), but in a small part of the second-order relativistic shift as well as in the finite mass effect, a required numerical calculation for $n=3$ has not yet been done. We have assumed the validity of the $1/n^3$ law for these cases and do not expect a numerically significant departure from it. The average excitation energies $k_0(n,l)$ which occur in the logarithm have been calculated by Harriman.[10] The separation $\Sigma(3\,^2P_{\frac{3}{2}}-3\,^2D_{\frac{3}{2}})$ has theoretical contri-

[10] J. M. Harriman, Phys. Rev. **101**, 594 (1956).

butions listed in Table I(b). All other terms are negligible for present purposes. The doublet separations are caused by interaction of the electronic magnetic moment and orbital motion. The contributions to $\Delta E(3\,^2P_{\frac{3}{2}}-3\,^2P_{\frac{1}{2}})$ and to $\mathfrak{D}E(3\,^2D_{\frac{5}{2}}-3\,^2D_{\frac{3}{2}})$ are shown in parts c and d of Table I.

4. Comparison with Spectroscopic Observations

Measurements of $n=3$ fine structure have been made by Series,[2] whose latest work gives $\mathcal{S}=250_{-90}{}^{+60}$ Mc/sec. This result is in very mild disagreement with the theoretical value. There is recent evidence, moreover, that the corresponding shift for $n=4$ of He^+ is in better accord with theory than $n=3$ of H despite earlier evidence to the contrary.[11] Possibly the spectroscopic observations are complicated by just the same anomalous intensities of fine structure components which make possible the present experiment.

5. Lifetimes of States and Radiative Widths of Resonances

Table II shows the computed lifetimes for the radiative decay of isolated atoms in $2s$, $2p$, $3s$, $3p$, and $3d$ states. The atomic beam experiments of Lamb and Retherford for $n=2$ depended on the metastability of $2s$, but the life of $3s$ is too short to permit formation of a beam of slow atoms in $3s$. On the other hand, the conditions are suitable for a microwave-optical experiment, as discussed in Sec. 1, since with equal rates of excitation of all sublevels, the steady state population of a $3s$ sublevel would be 30 times that of one for $3p$. There would also be a significant departure from equipartition for $3p$ and $3d$.

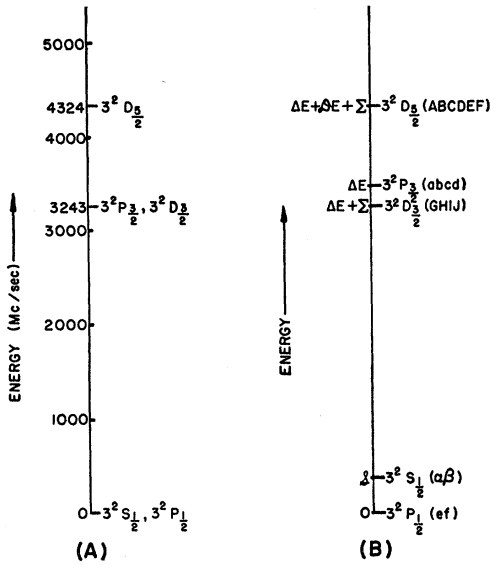

FIG. 1. The $n=3$ levels of H atoms (A) according to Dirac theory, (B) in the notation of this paper. The various sublevels belonging to each fine structure level are indicated in parentheses (in order of decreasing magnetic quantum number).

[11] G. W. Series, Proc. Roy. Soc. (London) **A226**, 377 (1954); G. Herzberg, Z. Physik **146**, 269 (1956). For a review of the spectroscopic measurements see G. W. Series, *The Spectrum of Atomic Hydrogen* (Oxford University Press, New York, 1957).

TABLE II. Radiative lifetimes of some excited states of H atoms.

n	State	Radiative lifetime (sec)	Reference
2	$2s$	0.12	a
	$2p$	1.6×10^{-9}	b
3	$3s$	1.6×10^{-7}	b
	$3p$	5.4×10^{-9}	b
	$3d$	1.6×10^{-8}	b

[a] J. Shapiro and G. Breit, Phys. Rev. **113**, 179 (1959).
[b] H. A. Bethe, *Handbuch der Physik*, edited by S. Flügge (Verlag Julius Springer, Berlin, 1933), Vol. 24, Part 1.

According to Eq. (6) the radiative width at half height of a resonance corresponding to states a and b is $(\gamma_a+\gamma_b)$ in circular frequency units. The corresponding widths for $3s-3p$ and $3d-3p$ resonances are 30.5 Mc/sec and 39.5 Mc/sec, respectively.

6. Zeeman Effect of Fine Structure

For reasons which have become familiar, the experiment is carried out in a magnetic field. The $3s$, $3p$, and $3d$ states are not mixed in Zeeman splitting and one can discuss each separately.[12]

The effective Hamiltonian for $3s$ states is

$$\mathcal{S}+g_s\mu_0\mathbf{S}\cdot\mathbf{H},$$

where the Landé factor for spin is

$$g_s=2(1+\alpha/2\pi-0.328\alpha^2/\pi^2). \tag{21}$$

For $3p$ states, the effective Hamiltonian is

$$\tfrac{2}{3}\Delta E(1+\mathbf{L}\cdot\mathbf{S})+g_s\mu_0\mathbf{S}\cdot\mathbf{H}+g_L\mu_0\mathbf{L}\cdot\mathbf{H},$$

since $\mathbf{L}\cdot\mathbf{S}$ has eigenvalues -1 and $+\frac{1}{2}$ for $^2P_{\frac{1}{2}}$ and $^2P_{\frac{3}{2}}$, respectively. For $3d$, one has an operator

$$\Delta E+\Sigma+\tfrac{2}{5}\mathfrak{D}E(\tfrac{3}{2}+\mathbf{L}\cdot\mathbf{S})+g_s\mu_0\mathbf{S}\cdot\mathbf{H}+g_L\mu_0\mathbf{L}\cdot\mathbf{H},$$

since $\mathbf{L}\cdot\mathbf{S}$ has eigenvalues $-\frac{3}{2}$ and $+1$ for $^2D_{\frac{3}{2}}$ and $^2D_{\frac{5}{2}}$, respectively. The Landé factor for orbital motion is

$$g_L=1-m/M_D. \tag{22}$$

As a generalization of the notation used for $n=2$, we denote magnetic sublevels for $3s$ by letters α and β; for $3\,^2P_{\frac{3}{2}}$ by a, b, c, d; for $3\,^2P_{\frac{1}{2}}$ by e, f; for $3\,^2D_{\frac{5}{2}}$ by A, B, C, D, E, F with G, H, I, J used for $3\,^2D_{\frac{3}{2}}$.

The energies of these 18 states in a magnetic field are given by the equations:

$$E_{\alpha,\beta}=\mathcal{S}\pm\tfrac{1}{2}g_s\mu_0H, \tag{23}$$

$$E_{a,d}=\Delta E\pm(g_L+\tfrac{1}{2}g_s)\mu_0H, \tag{24}$$

$$E_{b,c}=\tfrac{1}{2}\Delta E\pm\tfrac{1}{2}g_L\mu_0H+\tfrac{1}{2}\lfloor(\Delta E)^2\pm\tfrac{2}{3}\Delta Eg\mu_0H+(g\mu_0H)^2\rfloor^{\frac{1}{2}}, \tag{25}$$

[12] The necessary theory is given in L.R.-III.

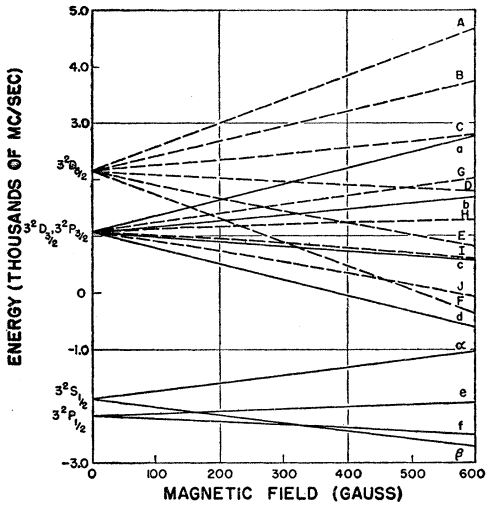

FIG. 2. The energies of $n=3$ sublevels of hydrogen as a function of magnetic field strength. The zero-field splittings are those predicted by quantum electrodynamics.

$$E_{e,f}=\tfrac{1}{2}\Delta E\pm\tfrac{1}{2}g_L\mu_0H-\tfrac{1}{2}[(\Delta E)^2\pm\tfrac{2}{3}\Delta Eg\mu_0H+(g\mu_0H)^2]^{\frac{1}{2}}, \quad (26)$$

$$E_{A,F}=\Delta E+\Sigma+\mathfrak{D}E\pm\mu_0H(2g_L+\tfrac{1}{2}g_s), \quad (27)$$

$$E_{B,E}=\Delta E+\Sigma+\tfrac{1}{2}\mathfrak{D}E\pm\tfrac{3}{2}g_L\mu_0H+\tfrac{1}{2}[(\mathfrak{D}E)^2\pm(6/5)\mathfrak{D}Eg\mu_0H+(g\mu_0H)^2]^{\frac{1}{2}}, \quad (28)$$

$$E_{G,J}=\Delta E+\Sigma+\tfrac{1}{2}\mathfrak{D}E\pm\tfrac{3}{2}g_L\mu_0H-\tfrac{1}{2}[(\mathfrak{D}E)^2\pm(6/5)\mathfrak{D}Eg\mu_0H+(g\mu_0H)^2]^{\frac{1}{2}}, \quad (29)$$

$$E_{C,D}=\Delta E+\Sigma+\tfrac{1}{2}\mathfrak{D}E\pm\tfrac{1}{2}g_L\mu_0H+\tfrac{1}{2}[(\mathfrak{D}E)^2\pm\tfrac{2}{5}\mathfrak{D}Eg\mu_0H+(g\mu_0H)^2]^{\frac{1}{2}}, \quad (30)$$

$$E_{H,I}=\Delta E+\Sigma+\tfrac{1}{2}\mathfrak{D}E\pm\tfrac{1}{2}g_L\mu_0H-\tfrac{1}{2}[(\mathfrak{D}E)^2\pm\tfrac{2}{5}\mathfrak{D}Eg\mu_0H+(g\mu_0H)^2]^{\frac{1}{2}}, \quad (31)$$

where $g=g_S-g_L$. The energies of the $n=3$ levels and the corresponding frequencies of transitions produced by a radiofrequency electric field perpendicular to **H** are shown in Figs. 2 and 3.

7. Hyperfine Energy

For simplicity, we consider the case of deuterium instead of hydrogen, since the hyperfine structure interactions, which are only an undesirable complication for fine structure studies, are much smaller for the heavier isotope.

The theory of hyperfine structure for $n=3$ of deuterium can be readily adapted from previous work (L.R.-III). It is convenient to use the zero field hyperfine splitting for $3s$, denoted by Δw, as a unit of energy. Apart from a negligible relativistic binding correction, this is just 8/27 of the corresponding $2s$ splitting[13] of 40.924 Mc/sec, i.e., $\Delta w=12.127$ Mc/sec.

[13] H. A. Reich, J. Heberle, and P. Kusch, Phys. Rev. **104**, 1585 (1956).

The hyperfine energy for the $3s$ states may be expanded for $\mu_0H\gg\Delta w$ as

$$w=\tfrac{2}{3}(\Delta w)m_Im_s-g_I\mu_0Hm_I+(4/9)[(\Delta w)^2/(2g_s\mu_0H)]\times[(2-m_I^2)m_s-\tfrac{1}{2}m_I]. \quad (32)$$

For the $3\,^2P_J$ states, the hyperfine energy for $\Delta E\gg\mu_0H\gg\Delta w$ is

$$w=\tfrac{1}{6}(\Delta w)m_Im_J/J(J+1). \quad (33)$$

All terms of order $(\Delta w)^2/\mu_0H$ are negligible for $H\geqq100$ gauss. For small departures from Russell-Saunders coupling, i.e., $\mu_0H\ll\Delta E$ there is a correction to w of

$$\pm(1/54)(\Delta w/\Delta E)\mu_0Hm_I,$$

but the only effect of this term for transitions $3s\leftrightarrow3p$ is a negligible change in the effective width of the composite resonance curves.

8. Matrix Elements of r for $n=3$

The matrix elements of $\mathbf{r}=(x,y,z)$ for transitions $3s\rightarrow3p$ and $3p\rightarrow3d$ are needed for calculation of the

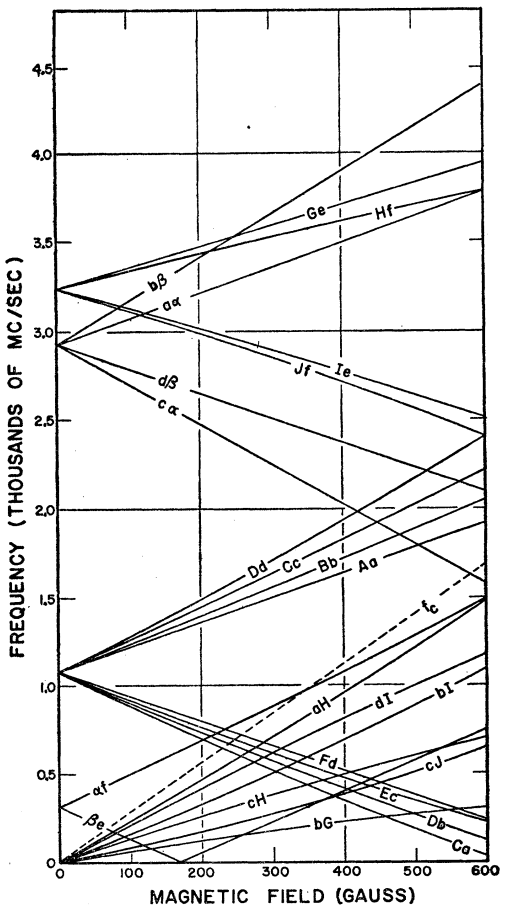

FIG. 3. The frequencies of the transitions (obeying $|\Delta L|=1$, $|\Delta m|=1$) plotted versus magnetic field. f_c is the electron cyclotron frequency.

amounts of rf power required to saturate the various transitions, and also to permit an estimate of the Stark shifts of levels due to various types of perturbing electric fields. The elements will be calculated in Russell-Saunders coupling which is suitable for magnetic fields satisfying $\mu_0 H \ll \Delta E$ for $3\,^2P$ or $\mu_0 H \ll \mathfrak{D} E$ for $3\,^2D$. Any corrections to this approximation which are significant numerically will be made when needed. Values of the quantities

$$|(n'l'j'm'|\mathbf{r}|nljm)|^2 \quad \text{for} \quad n=n'=3$$

can be readily obtained from equations given by Condon and Shortley,[14] and are listed in Table III in units of a_0^2.

For 50% saturation of a resonance, according to Sec. 1, it is required that the rf transition matrix element

$$V=e\mathbf{E}\cdot\mathbf{r}_{ab}/\hbar, \tag{18}$$

satisfy

$$|V|^2=\gamma_a\gamma_b. \tag{34}$$

For transitions αa, βb, and αe, the required rf electric field amplitudes are 0.82, 1.4, and 1.0 volts/cm, respectively.

9. Stark Effect

The susceptibility of excited states of hydrogen to electric field perturbations increases strongly with n. In the experiment of Lamb and Retherford with $n=2$ the main perturbing electric field was induced by the motion of the atoms at right angles to an applied magnetic field. Fields due to contact potentials played a relatively minor role. In the present experiment the excited atoms are necessarily studied in the electronic bombardment region. Among additional sources of perturbation are: macroscopic electric fields due to charges on the glass walls of the excitation tube, space charge due to electrons (which may be more or less neutralized by positive ions), and microscopic electric

TABLE III. Values of squared matrix elements $|(3l'j'm'|\mathbf{r}|3ljm)|^2$ in units of a_0^2. The transitions are designated according to the scheme adopted in Sec. 6 of this paper.

Transitions ij		$\lvert(i\lvert x\rvert j)\rvert^2=\lvert(i\lvert y\rvert j)\rvert^2$	$\lvert(i\lvert z\rvert j)\rvert^2$
aA	dF	81/4	0
aB	dE	0	81/5
aC	dD	81/40	0
aG	dJ	0	81/20
aH	dI	27/20	0
bB	cE	243/20	0
bC	cD	0	243/10
bD	cC	243/40	0
bG	cJ	27/20	0
bH	cI	0	27/60
bI	cH	27/15	0
eG	fJ	135/8	0
eH	fI	0	45/2
eI	fH	45/8	0
αa	βd	27	0
αb	βc	0	36
αc	βb	9	0
αe	βf	0	18
αf	βe	18	0

[14] E. U. Condon and G. H. Shortley, *The Theory of Atomic Spectra* (Cambridge University Press, Cambridge, 1951), p. 69.

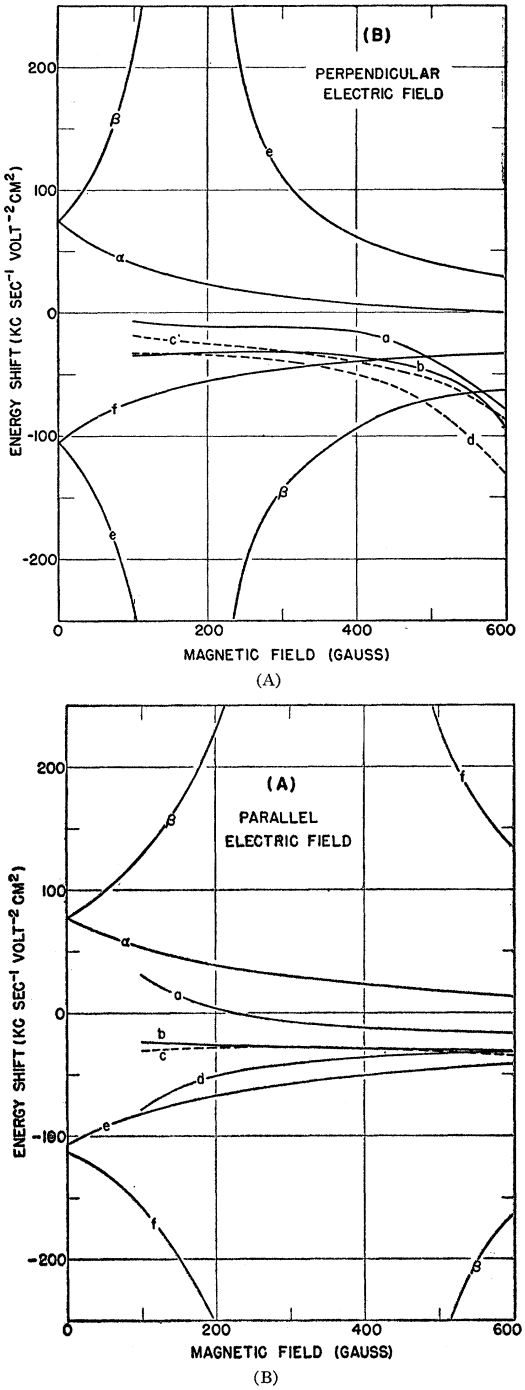

FIG. 4. Stark-effect shifts of sublevels of $n=3$ hydrogen for an electric field of strength 1 volt cm^{-1}. (A) For **E** parallel to **H**; (B) for **E** perpendicular to **H**.

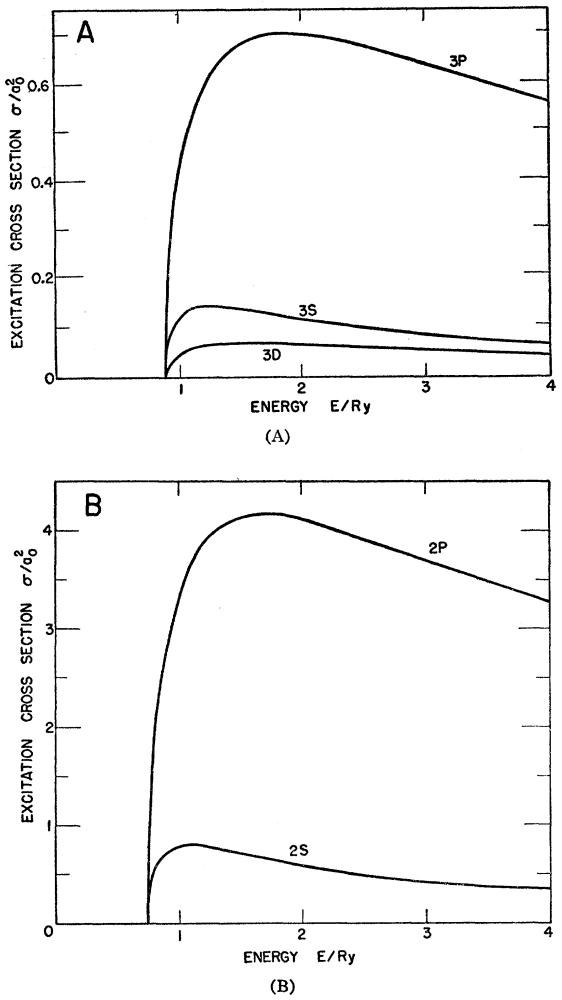

FIG. 5. Excitation cross section, in units of a_0^2, from the ground state of H atoms to the various $n=2$ and $n=3$ levels as calculated in Born approximation. The calculated cross sections given in Fig. 6 of L.R.-I are not correct.

fields due to electrons and positive ions. Despite the complexity of the situation, it will be shown in the following paper that some experimental limits can be set on the errors in energy level determination which can be caused by these effects.

In this section we will calculate the shifts caused by a macroscopic electric field E and postpone the quantitative application of the results to the following paper. As in Sec. 57 of L.R.-III, the second-order Stark shift of level i of unperturbed energy E_i is

$$\Delta E_i=-\sum_n |(n|e\mathbf{E}\cdot\mathbf{r}|i)|^2/(E_n-E_i). \quad (35)$$

The behavior near crossing points where an unperturbed energy $E_n=E_i$ requires a special treatment also to be given in the following paper. The shifts for some levels of interest as calculated from Eq. (35) for an electric field of one volt/cm are shown in Fig. 4.

10. Excitation Cross Sections for $3s$, $3p$, and $3d$

Success of the experiment depends in part on production of a difference in steady-state populations of the two levels a and b between which transitions are induced by rf. Fortunately, however, conditions are favorable in this respect. Since the lifetime of $3s$ is thirty times that of $3p$, the excitation cross section for a sublevel of $3p$ would have to be closely equal to thirty times that for $3s$ in order to give an effective cancellation of the factor $(r_a/\gamma_a)-(r_b/\gamma_b)$ in Eq. (4). Even if this factor were to vanish for one bombarding energy, it could hardly do so for all energies.

Although the Born approximation cross sections for excitation of atoms are not very reliable, the results predicted on this basis are shown in Figs. 5(A) and 5(B) for $n=2$ and $n=3$. The peak cross sections, summed over all sublevels, are $0.14a_0^2$, $0.7a_0^2$, and $0.07a_0^2$, for $3s$, $3p$, and $3d$, respectively. Even if we ignore the complication that the sublevels may be unequally excited in electron bombardment, there is no indication that the population difference factor of Eq. (4) is likely to vanish.

All the methods of production of hydrogen atoms which were discussed in L.R.-I have the disadvantage that they produce background light at the Balmer wavelength. Consideration was therefore given to the possibility that atoms in $n=3$ states could be produced directly by electron bombardment of hydrogen molecules. Some information about the corresponding process for $n=2$ was available from the work of Lamb and Retherford.[15] It was shown there that despite a weak violation of the Franck-Condon principle, metastable hydrogen atoms could be produced by electron bombardment above a threshold of 14.7 ev. For $n=3$, this figure should be raised by 1.9 ev. The dissociation products $H(1s)+H(3s,3p,3d)$ would separate completely in a radiative decay time so that the fine structure levels would be characteristic of atoms rather than molecules. With this method, however, the excitation cross sections are even harder to calculate, but the 18 sublevels should be more nearly in equipartition. The experimental simplicity of a direct process led us to try the molecular bombardment method before going on to a two-step mechanism.

Calculations by Harriman[16] indicate that about 4.4% of electronic excitations which ionize the H_2 molecule lead to the formation of slow protons. These have a rapidly falling energy distribution with only 50% of the protons having kinetic energies above 0.22 ev. One may expect to find that about an equal percentage of electronic excitations to $n=3$ molecular levels will lead to dissociation with production of slow atoms in $n=3$ states. The low efficiency of the process suggests that in later work the two-step process might be attempted.

[15] L.R.-II, Sec. 42.

[16] J. M. Harriman, Ph.D. dissertation, Stanford University (unpublished).

The velocity distribution of excited hydrogen atoms is of interest because of the motional Stark effect as discussed in L.R.-III and in Sec. 9. Deuterons having a kinetic energy of 1 ev would have a speed of 0.98×10^6 cm/sec. Moving across a magnetic field of 100 gauss they would experience a motional electric field of 0.98 volt/cm. Hence, the change in frequency for the αa transition should be 0.047 Mc/sec for these deuterons, and the Stark effect is negligible.

For bombarding energies greater than 28 volts, transitions to a repulsive molecular electronic state can be produced. One then expects some formation of excited $n=3$ atoms with about 6 ev of kinetic energy. Here no violation of the Franck-Condon principle is involved, but since the electronic excitation involves both molecular electrons, the cross section should be at most comparable with that for slow atoms in the $n=3$ states. The relative yields of fast and slow excited atoms will be discussed in the following paper from an experimental point of view.

11. Size of Signal Expected

From the foregoing we may estimate the intensity of H_α light emitted when an electron beam traverses a region filled with molecular hydrogen. We may further calculate the change in light intensity produced by application of a radio-frequency electric field. If I is the electron current, ρ_H the number density of hydrogen molecules, l the length of the interaction space, and σ_s, σ_p, and σ_d the cross sections for excitation of $n=3$ levels from molecular hydrogen (summed over sublevels in each case), we have

$$r'(0)=(f_s\sigma_s+f_p\sigma_p+f_d\sigma_d)(\rho_H lI/e); \tag{36}$$

$r'(0)$ is the total number of H_α quanta emitted per second from all $n=3$ levels. Now $f_s=f_d=1$, $f_p=1/8.5$. Inserting numbers typical of our experimental conditions,

$$I/e=6.25\times10^{14}\ \text{sec}^{-1}\ (100\ \text{microamp}),$$
$$\rho_H=3.6\times10^{13}\ \text{cm}^{-3}\ (10^{-3}\ \text{mm pressure}),$$
$$l=1\ \text{cm},$$

yields

$$r'(0)=(1/a_0^2)(\sigma_s+\sigma_p/8.5+\sigma_d)\times6.2\times10^{11}\ \text{sec}^{-1}. \tag{37}$$

If we arbitrarily set the bracketed expression equal to 10^{-18} cm^2 we obtain $r'(0)=2.5\times10^{10}$ sec^{-1}. The number of H_α quanta reaching the detector per second is $r_d(0)=\eta\cdot r'(0)$, where η is the light collecting efficiency of the optical system. Taking $\eta=0.1$ as fairly typical, we obtain

$$r_d(0)=2.5\times10^9\ \text{sec}^{-1}. \tag{38}$$

We now estimate the change in H_α intensity expected upon application of a radio-frequency field. Considering an rf transition between two states, a and b, we may write

$$r'(0)=f_a r_a+f_b r_b+r''(0), \tag{39}$$

where $r''(0)$ is the rate of emission of H_α light from states other than a and b. For large radio-frequency field strength, i.e., that sufficient to produce 100% saturation, we obtain a signal of magnitude

$$r(R)-r(0)=S=-(f_a-f_b)[(r_a/\gamma_a)-(r_b/\gamma_b)]\times(\gamma_a\gamma_b)/(\gamma_a+\gamma_b), \tag{40}$$

as follows from Eq. (4) or (6).

If a is a $3s$ sublevel, and b a $3p$ sublevel, we have $(f_a-f_b)=0.88$ and assuming $r_a/\gamma_a\gg r_b/\gamma_b$ and $\gamma_b\gg\gamma_a$, we obtain

$$S=-0.85r_a, \tag{41}$$

where r_a is equal to the rate of excitation at a single sublevel of the $3s$ state. To relate the signal to the total intensity of H_α light we need some information regarding the relative excitation cross sections for $3s$, $3p$, and $3d$ sublevels. Lacking such detailed information for the direct excitation from the molecule we assume equal excitation cross sections for each Zeeman sublevel of $n=3$. Thus we derive

$$r(0)=(2f_s+6f_p+10f_d)r_a=12.7r_a. \tag{42}$$

Finally, substitution of (41) in (42) yields

$$S=-0.07r(0), \tag{43}$$

that is, application of a large rf electric field produces a seven percent decrease in the intensity of H_α emission from the electron bombarder. Using our estimate (38) that in the absence of rf the flux of H_α quanta at the detector is 2.5×10^9 sec^{-1}, we predict an rf-induced decrease of 1.7×10^8 sec^{-1}. For "optimum" rf field strength as defined in Sec. 1, the signal is reduced relative to the completely saturated value by a factor of one-half.

12. Observation of the Transitions

At the time these measurements were begun, the RCA 6217 photomultiplier seemed the best available detector for H_α light. The manufacturer's stated luminous sensitivity corresponds to a quantum efficiency of approximately 1% at 6563 A. Thus if we write r_e for the number of photoelectrons per second leaving the photocathode and S_e for the rf-induced change in this number, (38) and (43) predict the values

$$r_e=2.5\times10^7\ \text{sec}^{-1}, \tag{44}$$

$$S_e=1.7\times10^6\ \text{sec}^{-1}. \tag{45}$$

The main source of noise in the system may be expected to be shot noise at the photocathode. If we write τ(sec) for the time over which current is averaged, the estimated signal-to-noise ratio S/N is

$$\frac{S}{N}=\frac{1.7\times10^6\tau}{(2.5\times10^7\tau)^{\frac{1}{2}}}=340\tau^{\frac{1}{2}}, \tag{46}$$

provided that the steady H_α light r_d is larger than any

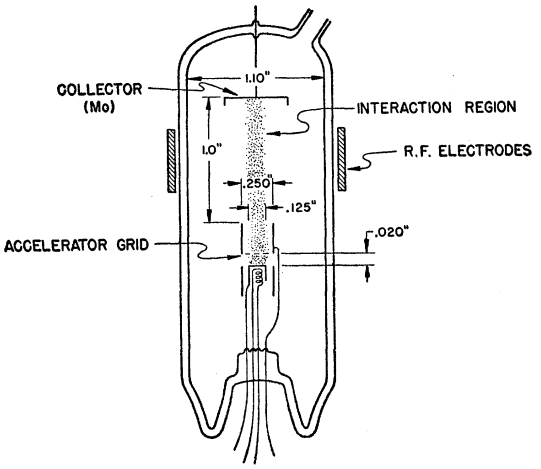

FIG. 6. The MkI electron bombarder.

background light at the detector and that shot noise at subsequent stages of the multiplier and all other sources of noise in the system are negligible. If the ratio of background light to H_α light at the detector is ρ, (46) becomes

$$S/N=340\tau^{\frac{1}{2}}/(1+\rho)^{\frac{1}{2}}. \quad (47)$$

For $\rho\ll 1$ and $\tau=3$ sec, we predict

$$S/N\cong 600.$$

The radio-frequency power requirements may be readily estimated from the fields required for 50% saturation listed in Sec. 8. For $E_{rf}=1$ volt/cm and a matched transmission line of effective cross section 3 cm^2 approximately 12 milliwatts of rf would be required. This power is readily available over the frequency range of interest. Since it is convenient to be able to operate at widely different frequencies without major changes in the apparatus, it was decided to use an approximately matched transmission line.

The electron bombarder should be capable of supplying currents of at least 100 μa, and should include a region as nearly free of electric fields as possible, in which the radio-frequency field may be applied and from which emitted light may be detected. Red light from the cathode of the electron bombarder must be prevented from reaching the photomultiplier.

B. APPARATUS

13. Electron Bombarder

The electron bombarders used in all phases of the work were constructed so as to allow baking of the entire tube at temperatures of 400°C. This procedure was believed desirable to insure purity of the hydrogen and to allow cleaning up of internal surfaces of the bombarder to avoid the buildup of insulating layers on the walls and electrodes. Effects due to such charges can be very troublesome and have been discussed in connection with $n=2$ hydrogen in L.R. I and II. In addition to a bakeout at 400°C the internal metal electrodes of the tube were outgassed at higher temperature by the use of a low-power induction heater.

The earliest apparatus was designed so that the electron gun was completely demountable, the vacuum seal being made by a copper gasket between two 18-8 stainless-steel flanges. However, the first bona fide resonances were observed with a nondemountable electron bombarder, sealed into a Nonex (7720) glass envelope. Since this tube performed satisfactorily for a period of several months, the demountability feature seemed unnecessary and was abandoned. The work here described was performed on two nondemountable tubes, herein called MkI and MkII. The MkI glass tube is shown in Fig. 6. The pumping tube was located near the collector lead. All materials in the tube were nonmagnetic. The wolfram rods were spot-welded to flexible leads of Advance wire. The grid was obtained from Eitel-McCullough and is used in the type 2C39A vacuum tube. It is constructed of gold-plated 0.001-in. wolfram wires spaced 0.003 in. between centers and attached to a gold-plated wolfram ring. The grid structure was attached to a short Mo cylinder to prevent direct cathode light from reaching the detector. The cathode was a 3-mm Philips dispenser-type cathode which showed some tendency to poison and lose emission under the operating conditions in this apparatus. In operation the accelerator grid and the collector were held at the same potential, and the cathode current divided approximately equally between the two. The cathode was operated at the minimum temperature required to give the desired emission in order to minimize the stray cathode light arriving at the detector.

The MkII tube differed from this design in a few details. The cathode material in this tube was lanthanum boride deposited on carburized Mo. The dimensions of the cathode were made identical with those of the Philips cathode, and the same type of heater was used. The inner surface of the light baffling cylinder attached to the grid was blackened with a deposit of colloidal graphite to minimize light reflection. The collector was cup-shaped (opening toward the cathode) to prevent the detector from receiving cathode light reflected from the plane surface of the collector.

14. Gas Supply and Vacuum Systems

The MkI electron bombarder was operated in a kinetic vacuum system for a period of approximately three months. Hydrogen or deuterium could be admitted to the system through a heated Pd tube, the temperatures of the Pd being used to control the flow rate, hence the hydrogen pressure. When hydrogen was not entering the system, a vacuum of 1×10^{-7} mm Hg or lower was consistently obtained at the gauges, which were a CVC-type PHG-06 Philips gauge and a CVC VG1A ionization gauge. A CVC GF 25-W oil diffusion

pump, backed by a booster pump and a mechanical pump, exhausted the system and a large liquid nitrogen trap, whose capacity was sufficient to last over 24 hours, was kept filled at all times. The system was operated with indicated hydrogen and deuterium pressures of up to 2×10^{-3} mm Hg at the Philips gauge. (This figure includes the nominal change in gauge sensitivity for hydrogen listed by the manufacturer.)

The MkII electron bombarder was processed on this same vacuum system, but was sealed off from it with a Bayard-Alpert ionization gauge (WL-5966) and the Pd leak. This tube was baked out and rf heated and operated with electron emission while connected to the pumping system. The glass tubulation was then sealed off and deuterium was admitted through the palladium. Pressure control in the tube was possible since additional deuterium could be admitted by heating the palladium, and the hot wolfram filament of the ionization gauge proved to be an efficient pump for the hydrogen.

15. Light Detecting System

In order to reduce the background light at the detector to reasonable proportions, it was generally necessary to use a rather narrow-band optical filter. A Baird Associates Multilayer interference filter was used. In conjunction with a piece of red glass to eliminate a broad transmission peak in the blue, this system yielded a peak transmission of approximately 60%, and width at $\frac{1}{2}$ maximum of 75 A.

Since the electron bombarder operated in a magnetic field, and the photomultiplier must be kept away from such fields, it was necessary that the light from the interaction region be led at least six inches to the photomultiplier. Two systems were used for this purpose. One was a polished Lucite rod of 1-inch diameter, one end of which was in contact with the filters. The other end was placed nearly in contact with the outside of the electron bombarder envelope. Such a system has good light gathering power, but suffers from two disadvantages:

1. It collects unwanted light from remote parts of the electron bombarder.

2. Many of the light rays it gathers subtend rather large angles with the axis of the pipe. The wavelength transmission characteristics of the interference filters are considerably shifted for such oblique rays.

In most of the later work a lens system was used, giving good performance in spite of very limited light gathering ability. This system was a single lens with focal length equal to 1.5 in. and diameter 1 in. located approximately 2.25 in. from the electron beam. The lens was mounted in a well light-baffled brass tube of length 6 in. The image of the interaction region filled the output end of the tube, and more oblique rays struck the walls and were absorbed. The photomultiplier was shielded against the ambient magnetic field by a mumetal shield.

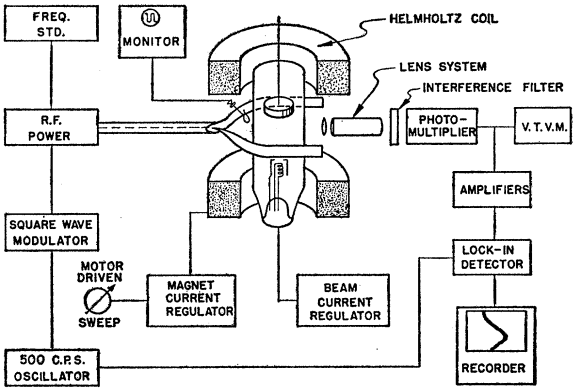

FIG. 7. A general schematic view and block diagram of the experimental apparatus.

16. Magnetic Field and Field Measurement

Magnetic fields up to 600 gauss were produced by a pair of Helmholtz-type coils. These coils were wound of No. 22 silicone enamel insulated wire on water-cooled brass spools. Regulated currents up to 1.5 amp were supplied by a selenium rectifier supply and an electronic regulator. Both current regulation and field homogeneity over the interaction region were in the neighborhood of one part in 5000.

Magnetic field measurement presented some difficulty in the MkI apparatus since it was not feasible either to place a field measuring probe in the interaction region or to move the electron bombarder and substitute such a probe. Accordingly, use was made of the electron cyclotron resonance, which had very prominent effects in the operation of the tube. This resonance appeared in the form of an increase in light output from the tube which was extremely strong and broad when excited by an rf field of amplitude appropriate for the hydrogen fine-structure resonances. Study of sharper cyclotron resonances under conditions of lower rf amplitude showed them to be subject to shifts of the order of their widths (0.2 gauss). These shifts, presumably due to inhomogeneous electric fields in the tube, appeared to vary with gas pressure, rf amplitude, and applied magnetic fields, making the cyclotron resonance unsuitable for accurate field determinations. When the MkII tube was installed, advantage was taken of its portability and a proton resonance probe, interchangeable with the electron bombarder, was used for magnetic field calibration. Magnetic field measurements were made by measurement of the current in the Helmholtz coils and calibration points were supplied by use of the proton resonance.

17. Radio-Frequency Sources and Fields

Radio-frequency fields were applied between two parallel plates, fed from a 50-ohm coaxial line via the crude tapered section shown in Fig. 7. With this arrangement it was possible to feed frequencies in the

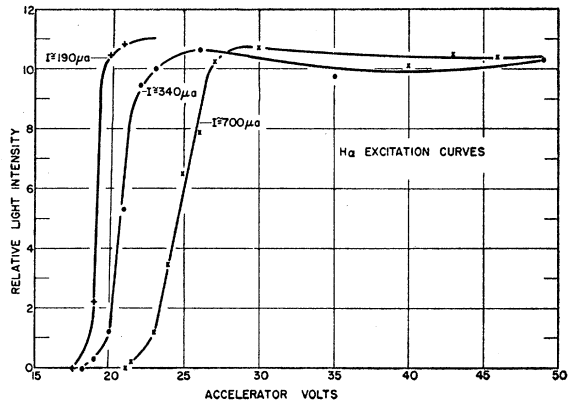

FIG. 8. Excitation curves, taken with the MkI electron bombarder. The pressure of molecular hydrogen was 4×10^{-4} mm Hg.

range 300 to 3500 Mc/sec into the system with a moderate VSWR when the parallel plate line was terminated in a 250-ohm deposited carbon resistor. A double stub tuner in the 50-ohm line was frequently used for matching purposes. A pickup loop mounted near the terminating resistance and a 1N23 crystal detector were used to monitor the rf level. The most careful measurements reported in the present paper were carried out in the wavelength region of 10 cm. WL417A klystrons were used as signal sources in this frequency region. For study of lower frequency resonances, including the electron cyclotron resonance, a variety of oscillators was used. A variable attenuator, consisting of a tapered lossy card inserted through a slot into a length of rigid 50-ohm coaxial line was employed to control the rf amplitude.

Proton resonance frequencies were measured with a BC 221-Q frequency meter, high frequencies with a TS 186/UP frequency meter. The internal crystals in these devices were found to be correct to better than 1 part in 10^5, sufficient for the present measurements.

18. Other Apparatus

Early attempts to find the resonances by varying the magnetic field and looking for changes in the direct current output of the photomultiplier indicated the desirability of an ac detection scheme. The broad resonances require that rather wide ranges of magnetic field be swept. The performance of the electron bombarder was somewhat sensitive to magnetic field variation and the photomultiplier was not perfectly shielded against magnetic fields. In addition, the filament temperature and therefore the background light were sensitive to variations in hydrogen pressure. All these effects caused variations in dc light which proved to be large compared to the effects of interest. A number of different modulation schemes are possible, of which two, modulation of the magnetic field and the radio-frequency amplitude were considered. Magnetic field modulation is not ideal in this experiment, since the variable sensitivity of the electron bombarder to magnetic field would cause a wandering base line which would have to be determined separately at each value of the magnetic field by turning the rf on and off. This being the case, it seemed more desirable simply to turn the rf on and off with a square wave. The ac component of photomultiplier output at the modulation frequency then indicates directly the change in light output caused by application of the rf. This modulation scheme is, of course, unsuitable if the required rf field strengths are sufficient to produce a "multipactor" or other light-producing discharge. The radio-frequency fields used in the present experiment (see Sec. 8) are sufficiently low that such effects ordinarily did not appear. Square wave modulation of the rf amplitude at 500.2 cps was provided by use of a square-wave modulated regulated power supply. This source was used as the plate power supply for the low-frequency oscillators, and a square wave was applied to the reflector electrode of the klystrons. This was of sufficient amplitude to drive a WL417A into and out of oscillation.

The source of the 500.2-cps signal was a resonant reed. The sinusoidal 500.2-cps wave was amplified and clipped and, as shown in Fig. 7, served for modulation and as a reference signal for a double-diode phase-sensitive detector. The signal from the photomultiplier, after preamplification, was applied to a Q multiplier which was operated with a bandwidth of a few cycles. After this preliminary narrow-banding, the signal was fed to the phase-sensitive detector. The output of the lock-in could then be displayed on a voltmeter or a recording potentiometer.

For study of the proton resonance, magnetic field modulation was used. A 500.2-cps sinusoidal current was applied to two modulating coils, and the audio output of an oscillating detector proton resonance system was fed to the same narrow-band amplifiers, lock-in detector, and recorder.

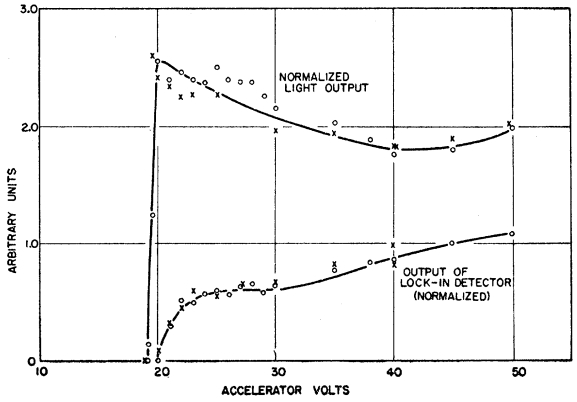

FIG. 9. H_α light intensity and strength of the αf resonance ($\nu=492$ Mc/sec) plotted against accelerating potential. MkI bombarder; $p=4\times10^{-4}$ mm Hg.

C. OBSERVATIONS

19. Characteristics of the Electron Bombarder

In order to understand conditions in the electron bombarder, studies were made of H_α light intensity and the strength of the rf-induced signal as functions of gas pressure and bombarding voltage. In the work described here, the understanding of the origin and magnitudes of electric fields within the interaction region was distinctly incomplete. Such subjects were studied in much greater detail prior to making more precise measurements and will be described in the following paper. The magnitude of these effects may be judged from the family of excitation curves shown in Fig. 8 which were obtained in the MkI electron bombarder. The shift and broadening of the threshold indicate a potential depression due to negative space charge on the inside of the electron beam. Excitation curves of this form are consistent with estimates of the potential variation within the electron bombarder assuming that no ion neutralization of electronic space charge occurs. Visual examination of the electron beam appeared to confirm the view, showing the threshold for light production to occur at lower accelerating voltages for the ends and edges of the electron beam than for the interior.

It is to be expected, however, that at bombarding voltages well above the threshold of 16.6 ev the ionization cross section will be large enough for considerable space charge neutralization to occur, with consequent reduction of macroscopic electric fields in the electron beam. This view is confirmed, to some extent, by the fact that in the MkI tube, where this situation prevailed, strong resonances were only observed for values of electron energy well above threshold. Figure 9 shows plots of αf resonance magnitude and light intensity versus accelerator voltage. Resonances were generally studied with accelerating voltage near 50 volts in the MkI bombarder. Under this condition the resonance

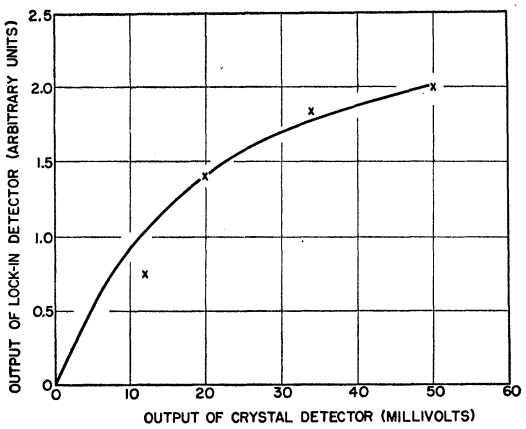

FIG. 10. A saturation curve for the αf resonance. The curve drawn is of the form predicted by Eq. (5), assuming the crystal voltage proportional to E^2.

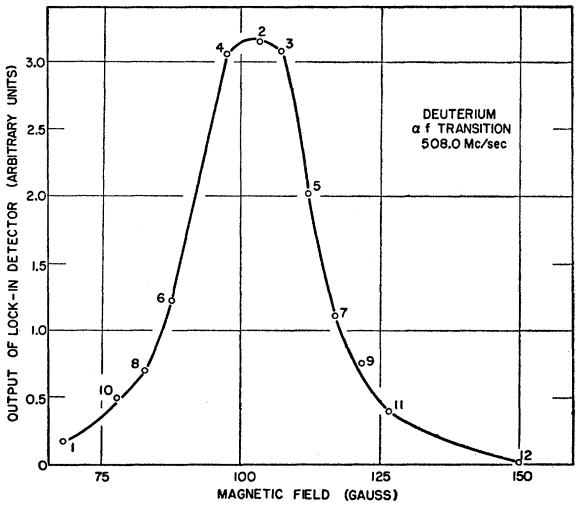

FIG. 11. The αf resonance in deuterium, MkI tube. The numbers beside the points indicate the order in which they were taken. The time required for the twelve points was approximately twenty minutes. The smooth curve has no theoretical significance.

amplitude appeared to be proportional to pressure and bombarding current for the values of these parameters studied, and showed the expected saturating dependence on rf amplitude. A plot of resonance amplitude versus open-circuit voltage at the crystal detector is shown in Fig. 10. The crystal might be expected to show some deviation from square law detection for the upper part of this curve, in such a direction that the true curve of resonance versus rf power would show more saturated behavior.

The MkII electron bombarder exhibited significantly different behavior. Excitation curves showed definite hysteresis, that is, the curve traced out when the accelerating voltage was raised differed from that observed when the voltage was decreased. Further, strong fine-structure resonances were observable with accelerating voltages as low as 21.5 volts.

20. Choice of "Operating Points"

As was true for the $n=2$ levels, the operating points, that is, the transition and frequency, must be chosen with care if accurate measurements are to be attempted. It is desirable to study transitions between levels far removed from other levels in order to minimize Stark-effect shifts. The level β is not suitable for precision work at any available field, "crossing" the e state near 165 oersteds, the f state near 320 oersteds. For the same reason states e and f should be avoided. The low-frequency transitions are further distorted by the presence of the electron cyclotron resonance which is extremely strong and broad, and rather near the αf resonance except in the weakest magnetic fields. These considerations mitigated against use of any low-frequency resonance for accurate measurement. The $^2P_{\frac{3}{2}}$ substates which may undergo rf transitions (obeying

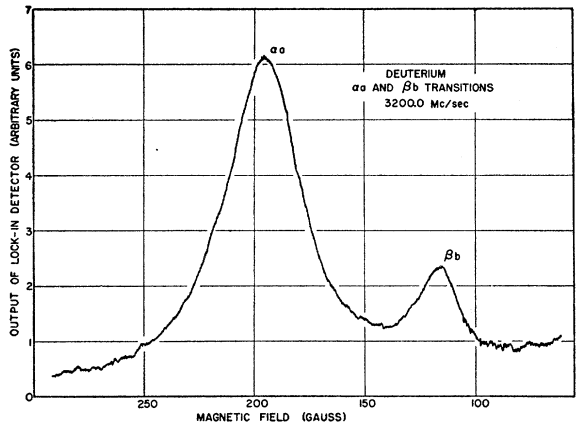

FIG. 12. Reproduction of recorder tracing of deuterium αa and βb resonances, MkII tube.

$\Delta m = \pm 1$) with α are a and c, of which a is considerably further from perturbing levels, except in the highest or lowest fields. State a has the additional convenient property of having a linear Zeeman effect. Transition αa was therefore selected for precision measurement.

In order to understand conditions in the interaction region it is convenient to study a resonance more sensitive to perturbing fields. This can be done when transitions involving the β level near a crossing point are observed. As was the case with the $n=2$ experiments,[17] anomalous resonances are observed near the βe crossing.

21. Resonances

Some representative resonances observed on the MkI and MkII systems are shown in Fig. 11 and Fig. 12. In qualitative agreement with the prediction of Sec. II, application of a radio-frequency field reduces the H_α light intensity by a few percent.

TABLE IV. Line center measurements, MkI system.

Gas	Transition	ν (Mc/sec)	Mag. field (gauss)	δ (Mc/sec)	$\Delta E-\delta$ (Mc/sec)
H	βe	573.8	484 ±7	319 ±12	
D	αf	482±5	89.1±1.5	315 ±8	
D	αf	508.0	102.2±1	316.8±2	
D	αa	3150.6	155.8		2932.5±7
D	αa	3522.0	421.0		2931.9±7

[17] L.R.-II, Sec. 47; L.R.-III, Part N.

22. Results

No correction will be made to the data in the present paper. The following article will consider the various perturbing fields in the apparatus and will apply necessary corrections to the measured resonances. Listed in Table IV are three resonances observed with the MkI system, and the values of δ and $(\Delta E-\delta)$ that may be derived from them. The quoted errors include those due to uncertainty in frequency and field measurement and in the location of the resonance centers, but do not take account of possible systematic shifts. Table V lists three measurements of the αa resonance under better conditions than those of Table IV. From these data the value $(\Delta E-\delta)_D=2934.5$ Mc/sec may be deduced. Assuming the theoretical value for ΔE of 3250.6 Mc/sec, one derives $\delta_D=316.3$ Mc/sec compared to a theoretical value of 315.33 Mc/sec. To the spread of the data of ±2 Mc/sec should be added an estimate of possible shifts in arriving at a limit of error for this figure. Since most conceivable Stark shifts will be produced by extremely inhomogeneous electric fields, varying from zero to a maximum value within the interaction space, one expects that a broadening comparable to the peak shift will result. Preliminary studies of the line shape showed no evidence of anomalous line broadening. Effects of the order of 10 Mc/sec would have been detected. Thus a preliminary figure, $(\Delta E_D-\delta_D)=2934.5\pm10$ Mc/sec seems appropriate.

TABLE V. Line center measurements, MkII system, deuterium αa resonance, $\nu=3200.0$ Mc/sec.

Magnetic field (gauss)	$\Delta E-\delta$ (Mc/sec)
191.2	2932.4
188.3	2936.4
188.8	2935.4
190.6	2933.2
	Average $\Delta E-\delta=2934.5$ Mc/sec

ACKNOWLEDGMENTS

We are indebted to M. Goodwin, B. Stuart, K. Machein, and J. Lee for the construction of parts of the experimental apparatus. The assistance of L. Wilcox in the later experimental work is also gratefully acknowledged.